Development of Y_2O_3 dispersion strengthened Cu alloy using Cu_6Y and Cu_2O addition through the MA-HIP process

Bing Ma[1], Yoshimistu Hishinuma[*1, 2], Hiroyuki Noto[1, 2], Yusuke Shimada[3] and Takeo Muroga[1, 2]

[1] *The Graduate University for Advanced Studies, Toki, Gifu, 509-5292, Japan*

[2] *National Institute for Fusion Science, Toki, Gifu, 509-5292, Japan*

[3] *Institute for Materials Research, Tohoku University, Sendai, Miyagi, 980-8577, Japan*

Abstract

A copper-based material is the recent main trend of advanced heat sink materials for the solid divertor systems, providing an optimal combination of excellent mechanical strength and superior thermal conductivity under severe neutron irradiation environment. In particular, oxide dispersion strengthened Cu (ODS-Cu) alloy with yttrium oxide (Y_2O_3) nano-particles is one of the promising materials because of the lower influence of the particles on thermal conductivity and the higher resistance to coarsening of the particles due to their thermodynamic stability. The metal Y as the Y_2O_3 source has been used to fabricate ODS-Cu alloys in the previous work. In this study, we used the Cu_6Y intermetallic compound as the new Y source material to form Y_2O_3 particles during mechanical alloying (MA) followed by hot isostatic pressing (HIP) process, and successfully fabricated ODS-Cu alloy with Y_2O_3 nano-particles using the Cu_6Y compound. The effects of Cu_2O addition in this process as the oxidant material were also investigated. Y_2O_3 nano-particles with typical size of 30 nm were successfully formed into the Cu intra-grains and around grain boundaries, and the density of the Y_2O_3 nano-particles increased by the Cu_2O addition. Cu_2O addition promoted the oxidation of Y from the Cu_6Y compound, forming Y_2O_3 nano-particles.

Keywords: Cu alloy, ODS, Y_2O_3, Cu_6Y compound, MA-HIP

[Corresponding Author]:

Name: Yoshimitsu Hishinuma

Affiliation: National Institute for Fusion Science

Postal address: Oroshi 322-6, Toki, Gifu, 509-5292, Japan

Telephone number: +81-572-58-2315

Fax number: +81-572-58-2676

E-mail address: hishinuma.yoshimitsu@nifs.ac.jp

1. Introduction

The service environment of the divertor components for fusion reactor is very severe with both high heat flux and neutron irradiation. For example, the tungsten mono-block divertor for ITER is expected to extract a heat flux of 10 MW/m^2 in steady state and 20 MW/m^2 in transient states [1-3]. Even severer condition and environment will be expected for DEMO reactor. Developing an advanced material to provide an optimal combination of excellent mechanical strength and superior thermal conductivity is the main trend of heat sink materials for divertor systems. Various means have been investigated to achieve long-term high temperature mechanical strength with maintaining higher thermal conductivity. Among them, precipitation-strengthening and oxide dispersion-strengthening (ODS) were the most popular means for the mechanical strength improvement [4]. As the reference material for ITER, the CuCrZr alloy is one of the representative precipitation-strengthened materials with an operating temperature window ranging from 250℃ to 325℃ [5]. This alloy, however, was not suitable to use at temperature exceeding 300℃ because of the coarsening of the precipitates. The alumina (Al_2O_3) dispersion strengthened Cu alloy is the most famous dispersion-strengthened material due to the excellent mechanical strength with higher thermal conductivity. The Al_2O_3 dispersion strengthened Cu alloy was manufactured by a relatively simple process called “internal oxidation method” [6], and is commercialized as the Glidcop®. Since it is expected that the heat flux loaded to the divertor component will be increased drastically by the high performance of the fusion plasma, further higher mechanical strength under high temperature is required for the dispersion strengthened Cu alloy applied as the heat sink material. In particular, nano-sized oxide particle dispersion in the ODS steel contributed extremely to improve the mechanical strength at high temperatures and the neutron irradiation resistance. It was also necessary to form the further finer scaled and homogeneous dispersive particles in the dispersion strengthened copper alloy.

Recently, it is known that yttrium oxide (Y_2O_3) is more attractive as the dispersoids than the Al_2O_3 for the development of dispersion-strengthened copper alloys. Compared with Al_2O_3, Y_2O_3 is expected to be more suitable because of not only the lower solubility of Y element (less than 0.05 wt.% at 300℃)

in the Cu matrix [7], which is appropriate for maintaining high thermal conductivity, but also the thermodynamic stability of Y_2O_3 which enhances the resistance to coarsening [8]. The mechanical alloying (MA) is the primary fabrication method for Cu-Y_2O_3, because the lower solubility of Y in Cu matrix limits the use of internal oxidation method [9]. Many efforts have been devoted to develop the ODS-Cu alloy with Y_2O_3 particles by MA methods. R. Shabadi *et al.* investigated fabrication of the ODS-Cu alloy with Y_2O_3 using Friction Stir Processing (FSP), and evaluated the influence of Y_2O_3 particles on the thermal conductivity [10]. Kudashov *et al.* succeeded in producing the ODS-Cu alloy with Y_2O_3 particles by MA process at lower temperature, which was called "cryo-milling", and subsequent hot pressing methods [11]. Aghamiri *et al.* fabricated the ODS-Cu alloy with dispersed Y_2O_3 particles by addition of control agents, and investigated the influence of atmosphere during MA process on morphology and microstructure [12]. Carro *et al.* attempted to produce ODS-Cu with Y_2O_3 particles by different routes using vacuum induction melting, cryomilling and conventional milling before hot isostatic pressing (HIP) process [13]. In the case of the Y_2O_3 addition, Y_2O_3 particles were directly mixed into the Cu, and then they were dispersed in a Cu matrix.

On the other hand, since the Y element is known as one of the most active metals, we found that oxidation of Y to form Y_2O_3 particles during MA can be a promising method for the Y_2O_3 dispersions. Due to the feasibility of nano-particle formation by mechanochemical alloying through the pulverization and the chemical interaction [14], we succeeded in producing the ODS-Cu with Y_2O_3 nano-particles using pure Y metal powders as the Y source material by mechanochemical alloying through the MA-HIP process [15, 16]. On this MA-HIP process, in fact, the segregation of dispersive particles when Y_2O_3 was added directly was not observed [17].

Considering the Cu-Y solid solution phases were formed during the MA process between pure Y and Cu materials [18], the addition of Cu-Y pre-alloys from the beginning was expected to reduce the milling time and decrease the impurity contamination during MA process [19]. In addition, the brittleness of intermetallic compounds was generally suitable for efficient MA process [20]. For example, T. Graning et al. demonstrated that Fe_3Y was easier to dissolve and distribute in the steel

matrix than Y_2O_3, and addition of Fe_3Y can reduce the milling time and decrease the oxygen impurity [21, 22].

In this study, we investigated the effect of addition of Cu_6Y intermetallic compound as the new Y source material to form Y_2O_3 during MA-HIP process, in order to realize homogeneous distributed Y_2O_3 particle into the ODS-Cu matrix through efficient MA process. The microstructure and mechanical properties of the ODS-Cu with Y_2O_3 nano-particles during MA-HIP process was investigated. In addition, the effect of the Cu_2O addition as the oxidant during the MA-HIP process was investigated.

2. Experimental procedures

2. 1. Preparation of the Cu_6Y compound and the MA-HIP processed samples

The Cu_6Y intermetallic ingot was made from metal Cu foil and block (99.99%, purity), metal Y chips (99.9%, purity). Pure Cu and pure Y materials in the atomic ratio of 6/1 were adjusted and melted using high-purity Ar atmosphere arc-melting apparatus at National Institute for Fusion Science (NIFS). The arc-melting was carried out several times in order to make the homogeneous Cu_6Y melted buttons. After the arc-melting, Cu_6Y melted buttons were heat-treated at 600℃ for 100 hours in a vacuum for the solution heat treatment. The Cu_6Y melted buttons after heat treatment were crashed easily and formed Cu_6Y compound fine powders due to the solution heat treatment. The raw mixture powders having the Cu-5.74 wt% Cu_6Y were prepared to fabricate ODS-Cu alloy with 1.38 wt% Y_2O_3 particles.

First of all, the Cu_6Y powder as the Y source material to form Y_2O_3 particles was milled with Cu (99.99%, purity, -300 mesh) powder for 16 hours with a speed of 250 rpm in a planetary-type ball milling machine (Pulverisetee-5, Fritsch) in the high purity Ar atmosphere glove box at NIFS. The diameter of stainless steel balls used for the MA process was 5 mm and then the ball/powder ratio was selected to be 7/3 based on the previous works [15, 16]. In the second stage, 2.62 wt % of Cu_2O (99.9%, purity, -300 mesh) powder was added into the half-milled mixture powders, followed by milling for another 16 hours with the same parameters. The milled mixture powders after MA treatment of total 32 hours were put into the iron tube capsules and transferred into NIFS-Sealing Device filled with high purity Ar

atmosphere for the sealing operation [23]. The tube capsules were degassed at 500˚C for 1 hour to reach the pressure of below 0.1 Pa before clamping, followed by welding to keep the powders in a vacuum condition. During the HIP process, the tube capsules were heat-treated under a pressure of 150 MPa and at a temperature of 1000 ºC for 2 hours.

2.2. Microstructure, thermal property and mechanical hardness evaluations

The phase transition and microstructure of the Cu_6Y intermetallic compound powders was evaluated by the differential thermal analysis (DTA) and X-ray diffraction (XRD) method. DTA measurements were carried out using thermogravimetry-differential thermal analysis apparatus (TG-DTA, Rigaku TG8110) from 800℃ to 1000℃ with a rate of 2℃/min in pure argon gas flow. Alumina powders were chosen as standard reference sample during the DTA measurements. The XRD analysis was conducted on the Rigaku RINT-2200 diffractometer with Cu Kα radiation with the parameters of 40 kV and 40 mA.

Microstructure and morphology of the MA-HIP processed Cu alloy bulk samples without and with Cu_2O addition were evaluated by XRD apparatus and scanning electron microscope (SEM, JEOL JSM-5600) equipped with energy dispersive X-ray spectroscopy (EDX). In addition, thin sampling from a part of the MA-HIP processed Cu alloy bulk samples was carried out using the focused ion beam (FIB, Hitachi nano DUE'T NB5000) machine. After that, nanostructure of the thin FIB sample was observed using electron backscatter diffraction (EBSD) and scanning transmission electron microscope (TEM, JEOL JEM-2800) equipped with EDX. The relative densities were tested based on Archimedes' method by electronic densimeter (alfa mirage MDS-300) The Vickers Hardness of the MA-HIP processed Cu alloy bulk samples were evaluated at room temperature with a loading of 100 gf/mm^2 for 30 sec.

3. Results and discussions

3. 1. Possibility of the Cu_6Y compound as the Y source material for the Y_2O_3 nano-particles

Typical XRD pattern of the Cu_6Y intermetallic compound powders are shown in Fig. 1. The standard powder diffraction data of the $Cu_{5.38}Y_{0.80}$ intermetallic compound is also shown in Fig. 1. The

miniaturization of the Cu_6Y compound powder was caused easily by the hand crushing. We found that Cu_6Y compound had a high mechanical brittleness and could be formed finer powders. The X-ray diffraction peaks of Cu_6Y powders almost completely correspond to the powder diffraction data of $Cu_{5.38}Y_{0.80}$ compound. The slight variation of the Cu/Y ratio around 6/1 is because the hexagonal structured Cu_6Y phase could accommodate phases of various Cu:Y ratio [24]. The Cu_6Y compound powder in this study was mainly obtained in the form of the $Cu_{5.38}Y_{0.80}$ single phase.

DTA curves of the Cu_6Y compound powder under high purity Ar atmosphere is shown in Fig. 2. DTA curves with the temperature ramping from 800℃ to 1000℃ and dropping from 1000℃ and 800℃ are shown in Figs. 2 (a) and (b), respectively. In the temperature ramping process, the first endothermic transition of the DTA curve was observed at 886℃. This suggests that the Cu_6Y compound powder was phase changed at around 886℃. The endothermic transition of the DTA curve was also observed at 928℃ after the second endothermic transitions at 911℃, and the Cu_6Y compound powder was melted completely at 928℃. The small endothermic transition at 943℃ are believed to be caused by the disturbance of composition due to the non-equilibrium reaction.

In the temperature dropping process, the first exothermic transition of the DTA curve was observed at 929 ℃. This suggests that the solidification are conducted at this temperature. The final exothermic transition of the DTA curve was observed at 885 ℃, corresponding to the phase transformation. We found that these endothermic and exothermic transition behaviors corresponded to the Cu-Y system binary phase equilibrium diagram shown in Fig. 3 [25], in which the eutectic temperature between Cu and Cu_6Y phases is at 880℃. We found that the endothermic and exothermic transition of 885℃ and 886℃ in DTA curve indicated the eutectic transformation. On the other hand, the endothermic and exothermic transition of 928℃ and 929℃ in DTA curve showed the melting point of the Cu_6Y compound and it indicated critical surface of the solid-liquid boundary of the Cu_6Y phase. From the thermal property of Cu_6Y compound, we found that Cu_6Y compound was dissociated into high purity liquid phases of Cu and Y at around the estimated melting point of the Cu_6Y phase during the HIP

treatment, and the liquid Y component diffused into the Cu matrix. Finally, liquid Y component was able to act as Y source and also was contributed for the Y_2O_3 phase formation.

3. 2. Micro and nanostructure of the dispersion strengthened Cu-alloy using Cu_6Y compound

Typical backscattered electron (BSE) images of the cross-sectional area on the MA-HIP processed bulk samples without Cu_2O addition are shown in Fig. 4. There were many precipitates (light gray color phases) with aggregated morphology into the Cu matrix. According to the estimation of the atomic ratio from EDX analysis, these precipitates were identified to be various Cu-Y intermetallic compound phases. Once the MA processed powders using Cu_6Y compounds were activated during HIP treatment at 1000℃, the Cu_6Y compound was melted at this temperature and the liquid phase promoted the yttrium diffusion into Cu matrix. We found that Y_2O_3 particles in the Cu matrix were able to be formed by the chemical reaction between the activated yttrium and the dissolved oxygen in the copper matrix. For the bulk sample without Cu_2O addition, many Cu-Y intermetallic precipitates with aggregated morphology, shown in Fig. 4 by light gray phases, were formed from non-reactive yttrium due to the lack of oxygen supply based on the dissolved oxygen into Cu matrix. Various Cu-Y intermetallic precipitates solidified and aggregated during the cooling step of the HIP treatment from 1000℃.

Comparison of the XRD patterns between the bulk samples without and with Cu_2O addition is shown in Fig. 5. In the case of the sample without Cu_2O addition, three kinds of the diffraction peaks corresponded to the Cu, Y_2O_3 and Cu-Y compound were confirmed, supporting the BSE image shown in Fig.4. We found that Y_2O_3 phase could form in the Cu matrix using Cu_6Y compound as the Y source material for the sample without Cu_2O addition. However, there still had relatively higher diffraction peak of Cu-Y compound due to the non-reactive Cu_6Y compound. In the case of the sample with Cu_2O addition, the diffraction peaks of Cu and Y_2O_3 were confirmed, accompanied by the disappearance of the diffraction peaks of Cu-Y compound. This implies that the Cu_2O was one of the effective oxidant material to promote the Y_2O_3 phase formation using Cu_6Y compound as the Y source material for the ODS-Cu alloy.

The details of the Y_2O_3 phase formation in the MA-HIP processed ODS-Cu alloy using Cu_6Y compound were investigated. Comparisons of the detailed XRD patterns between the bulk samples without and with Cu_2O addition as the oxidant material is shown in Fig. 6. Interestingly, in the sample without Cu_2O addition, the cubic (a=b=c) and hexagonal (a=b≠c) structured Y_2O_3 crystals were formed. The lattice constants (a-axis) of the cubic and hexagonal structured Y_2O_3 crystals, estimated using Bragg's law, were 0.5264 and 0.3658 nm, respectively. Furthermore, the formations of trace amounts of metal yttrium and Cu-Y-O compounds were also confirmed. In the case of the sample with Cu_2O addition, only the cubic structured Y_2O_3 crystal without impurity phases was observed. Comparing the differences in the XRD pattern and the lattice constant of the Y_2O_3 crystal shown in Figs 5 and 6, we found that pure oxygen dissociated from Cu_2O material during HIP process under high temperature and pressure, and then the dissociated oxygen contributed to promote Y_2O_3 formation as the supplement of the dissolved oxygen in copper. Therefore, Cu_2O supplied effectively the deficient oxygen for the Y_2O_3 formation. In future, it is necessary to investigate optimization of the amount of Cu_2O addition.

In order to explore the microstructure and Y_2O_3 particle size distribution of the MA-HIP processed Cu alloy with Cu_2O addition, typical STEM image, EBSD map corresponding the inverse pole figure and Cu grain size distribution of the MA-HIP processed bulk sample with Cu_2O addition are shown in Figs. 7 (a), (b) and (c), respectively. From the EBSD mapping, we found that the ODS-Cu alloy prepared by MA-HIP process had a typical non-oriented polycrystalline structure. In addition, the Cu grains after HIP treatment showed a wide particle size distribution range from nano to micron orders, and the average Cu grain size was estimated to be approximately 480 nm. This value was much smaller than the average Cu grain size of the Glidcop® AL-15 (approximately 1 μm) [26]. It may be possible that the Y_2O_3 particles formed from Cu_6Y compound act as a pinning centers to suppress the grain growth of Cu particles during HIP treatment.

Typical STEM images and element distribution mapping of the MA-HIP processed bulk sample with Cu_2O addition as the oxidant material are shown in Fig. 8. The areas (a) and (b) in Fig. 8 indicate the microstructures of the Cu intra-grain and the area of grain boundaries between fine and coarse Cu

particles, respectively. We found that the many Y_2O_3 particles made from the Cu_6Y compound were formed in the Cu intra-grains and near the grain boundaries. The average Y_2O_3 particle size was obtained to be approximately 30 nm. The number density of Y_2O_3 nano-particles was estimated to be approximately 1.7×10^3 μm^3. The number density was similar to that of the commercial Glidcop® (Al-15) [26]. We concluded that Y_2O_3 nano-particles were successfully formed though MA and HIP process using Cu_6Y compound as the Y source material for Y_2O_3 formation.

3.3 Comparisons of the mechanical hardness between various ODS-Cu alloy materials

Since high number density of Y_2O_3 particles were formed in the Cu matrix, mechanical strength enhancement due to the oxide dispersion strengthening was expected. Before Vickers hardness testing, the relative densitys of sample without Cu_2O and with Cu_2O were obtained to be 98.18% and 98.80%, respectively, indicating that dense ODS-Cu were fabricated by this MA-HIP process. Comparisons of the Vickers hardness between MA-HIP processed samples and various Cu alloy materials is shown in Fig. 9. Vickers hardness test is an effective and convenient method to characterize the mechanical property of material. Vickers hardness of commercial pure Cu sample was obtained to be approximately 50 H_v. On the other hand, Vickers hardness of Glidcop® and MA-HIP processed Cu-Y_2O_3 alloys with Cu_2O addition were obtained to be approximately 110 $H_v$and 120 H_v respectively, which were much higher than that of pure Cu material. We confirmed that oxide dispersion into Cu matrix was effective to improve the mechanical strength.

Vickers hardness of the Cu-Y_2O_3 with Cu_2O addition was estimated to be 120 ± 30 H_v, which was higher than that of sample without Cu_2O (90 ± 20 H_v). This was caused by the increase of Y_2O_3 particle fraction in the Cu matrix due to the oxygen supply from Cu_2O. In addition, the average Cu grain size of the samples with Cu_2O addition shown in Fig. 7 is approximately 480 nm, which is much smaller than that of the Glidcop®. The small Cu grain size was also effective to improve the mechanical strength. In future, it will be important to optimize the amounts of Cu_6Y compound and Cu_2O addition for further improvement of the microstructure and the mechanical properties.

4. Conclusion

We successfully fabricated the ODS-Cu with 1.38 wt% Y_2O_3 nano-particles using Cu_6Y compound as the Y source material through MA-HIP process. Cu_6Y compound was transformed into liquid phase during HIP treatment and act as Y source for Y_2O_3 phase formation. The Cu_2O addition on the MA-HIP process was highly effective to increase Y_2O_3 particle formation. Y_2O_3 particles with average particle size of 30 nm were formed in the Cu intra-grains and the grain boundaries, and act as a pinning centers to suppress the grain growth of Cu particles during HIP treatment. Vickers hardness of ODS-Cu alloys was much higher than that of pure copper. This was caused by the Y_2O_3 dispersion and Cu grain growth suppression.

Acknowledgement

This study was supported financially and performed by the Fusion engineering research project in NIFS (UFFF022-4) and the general collaboration research program (KEMF152) in NIFS. A part of this study was also financially supported by JSPS KAKENHI Grant Number (16H02443).

References

[1] J. Bucalossi, M. Missirlian, P. Moreau, F. Samaille, et al., “The WEST project: Testing ITER divertor high heat flux component technology in a steady state tokamak environment”, Fusion Engineering and Design, **89**, 907-912.

[2] A. S. Kukushkin, H. D. Pacher, V. Kotov, G. W. Pacher and D. Reiter, “Finalizing the ITER divertor design: The key role of SOLPS modeling”, Fusion Engineering and Design, **86**, (2011), 2865–2873.

[3] B. Li, V. Krsjak, J. Degmova, Z. Wang, T. Shen, H. L, S. Sojak, V. Slugen and A. Kawasuso, “Positron annihilation spectroscopy study of vacancy-type defects in He implanted polycrystalline α-SiC”, Journal of Nuclear Materials, **535**, (2020), 152-180.

[4] G. J. Butterworth and C. B. A. Forty, "A survey of the properties of copper alloys for use as fusion reactor materials", Journal of Nuclear Materials, **189**, (1992), 237-276.

[5] S. A. Fabritsiev, S. J. Zinkle and B. N. Singh, "Evaluation of copper alloys for fusion reactor divertor and first wall components", Journal of Nuclear Materials, **233-237**, (1996), 127-137.

[6] G. Carro, A. Muñoz, B. Savoini, and M.A. Monge, "Fabrication and characterization of dispersion strengthened Cu-0.8%Y", Fusion Engineering and Design, **154** (2020), 111548.

[7] M. Li and S. J. Zinkle, "Radiation Effects in Copper and Copper Alloys for Fusion Applications", Comprehensive Nuclear Materials 2nd edition, **6**, (2020), 93-110.

[8] J. R. Groza, and J. C. Gibeling, "Principles of particle selection for dispersion-strengthened copper materials", Materials Science and Engineering: A, **171**, (1993), 115-125.

[9] M. S. Nagorka, C. G. Levi, G. E. Lucas and S. D. Ridder, "The potential of rapid solidification in oxide-dispersion-strengthened copper alloy development", Materials Science and Engineering: A, **142**, (1991), 277-289.

[10] R. Shabadi, M. N. Avettand-Fènoël, A. Simar, R. Taillard, P.K. Jain and R. Johnson, "Thermal conductivity in yttria dispersed copper", Materials and Design, **65**, (2015), 869–877.

[11] D. V. Kudashov, H. Baum, U. Martin, M. Heilmaier and H. Oettel, "Microstructure and room temperature hardening of ultra-fine-grained oxide-dispersion strengthened copper prepared by cryomilling", Materials Science and Engineering: A, **387-389**, (2004), 768-771.

[12] S. M. S. Aghamiri, N. Oono, S. Ukai, R. Kasada, H. Noto, Y Hishinuma and T. Muroga, "Microstructure and mechanical properties of mechanically alloyed ODS copper alloy for fusion material application", Nuclear Materials and Energy, **15**, (2018), 17-22.

[13] G. Carro, A. Muñoz, M. A. Monge, B. Savoini, R. Pareja, C. Ballesteros and P. Adeva, "Fabrication and characterization of Y_2O_3 dispersion strengthened copper alloys", Journal of Nuclear Materials, **455**, (2014), 655-659.

[14] E. G. Avvakumov and L. G. Karakchiev, “Mechanochemical synthiesis as a method for the preparation of nanodisperse particles of oxide materials”, Chemistry for sustainable development, **12**, (2004), 287-291.

[15] B. Huang, Y. Hishinuma, H. Noto, R. Kasada, N. Oono, S. Ukai and T. Muroga, “In-situ fabrication of yttria dispersed copper alloys through MA-HIP process”, Nuclear Materials and Energy, **16**, (2018), 168-174.

[16] B. Huang, Y. Hishinuma, H. Noto and T. Muroga, “Mechanochemical processing of Cu-Y_2O_3 alloy by MA-HIP for heat sink materials application”, Fusion Engineering and Design, **140**, (2019), 33-40.

[17] D. Zhou, X. Wang, W. Zeng, C. Yang, H. Pan, C. Li, Y. Liu and D. Zhang, “Doping Ti to achieve microstructural refinement and strength enhancement in a high volume fraction Y_2O_3 dispersion strengthened Cu”, Journal of Alloys and Compounds, **753**, (2018), 18-27.

[18] G. Carro, A. Muñoz, M.A. Monge, B. Savoini and R. Parej, “Microstructural and mechanical characterization of Cu-0.8 wt.% Y”, Fusion Engineering and Design, **98–99**, (2015), 1941–1944.

[19] S. Sheibani, A. Ataie, S. H. Manesh and G.R. Khayati, “Structural evolution in nano-crystalline Cu synthesized by high energy ball milling”, Materials Letters, **61**, (2007), 3204–3207.

[20] T. Graning, M. Rieth, J. Hoffmann and A. Maoslang, “Production, microstructure and mechanical properties of two different austenitic ODS steels”, Journal of Nuclear Materials, **487**, (2017), 348-361.

[21] T. Graning, M. Rieth and J. Hoffmann, “Microstructural investigation of an extruded austenitic oxide dispersion strengthened steel containing a carbon-containing process control agent”, Journal of Nuclear Materials, **516**, (2019), 335-346.

[22] H. Noto, T. Yamada, Y. Hishinuma and T. Muroga, “Effect of atmospheric control during MA-HIP process on mechanical properties of oxide dispersion-strengthened Cu alloy”, Fusion Engineering and Design, **124**, (2017), 1024–1027.

[23] I. Kimio, Q. Guojun, S. Mey and P. J. Spencer, “Evaluation of the phase diagram and thermochemistry of the Cu-Y system”, Calphad,, **14**, (1990), 377-384.

[24] ASM Alloy Phase Diagram Database, ASM International

[25] N. Simos, Z. Kotsina, E. Dooryhee et al., “200 MeV proton irradiation of the oxide-dispersion-strengthened copper alloy (GlidCop-Al15)”, Journal of Nuclear Materials, **516**, (2019), 360-372.

Figure captions

Fig. 1 Typical X-ray diffraction (XRD) patterns of the Cu_6Y compound powders as the Y source for the Y_2O_3 particle formation.

Fig. 2 Differential Thermal Analysis (DTA) curves of the Cu_6Y compound powders as the Y source for the Y_2O_3 particle formation. Figs. 2 (a) and (b) indicate the case of temperature ramping and dropping, respectively,

Fig. 3 Cu-Y system binary equilibrium phase diagram [25].

Fig. 4 Typical Back Scattering Electron (BSE) images of the surface region in the MA-HIP processed bulk samples without Cu_2O addition.

Fig. 5 Typical X-ray diffraction patterns of the MA-HIP processed bulk samples without and with Cu_2O addition as the oxidant material.

Fig. 6 Comparison of the detailed X-ray diffraction patterns after HIP process between the bulk samples without and with Cu_2O addition as the oxidant material.

Fig. 7 EBSD mapping and Cu grain size distribution of the MA-HIP processed bulk sample with Cu_2O addition as the oxidant material. (a) is the STEM image of the sampling area, (b) is the EBSD analysis corresponding the inverse pole figure, and (c) is the Cu grain size distribution estimated from the EBSD analysis.

Fig. 8 Typical STEM images and element distribution mapping of the MA-HIP processed bulk sample with Cu_2O addition as the oxidant material. (a) Cu intra-grain region, and (b) area of grain boundaries between fine and coarse Cu particles.

Fig. 9 Comparisons of the Vickers hardness of MA-HIP processed samples and various Cu alloy materials.

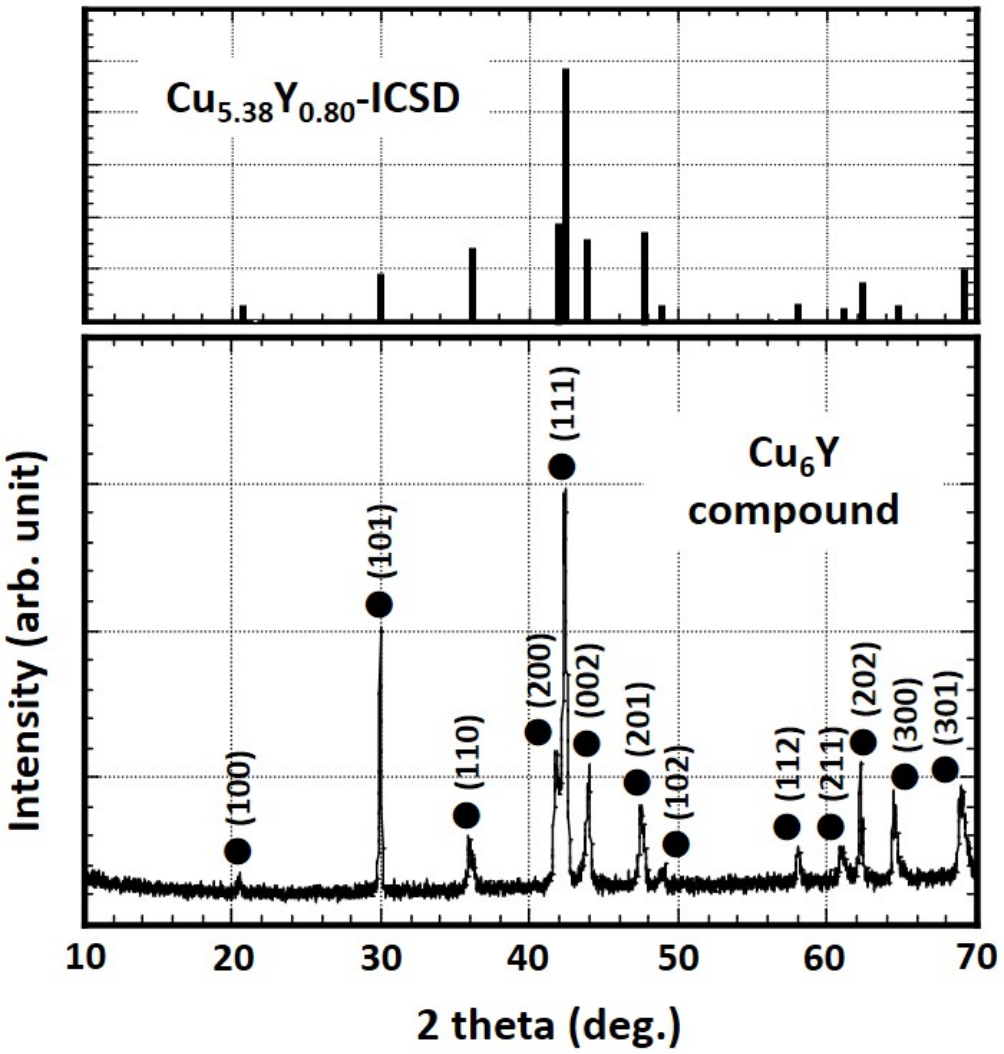

Figure.1 Bing Ma et al.

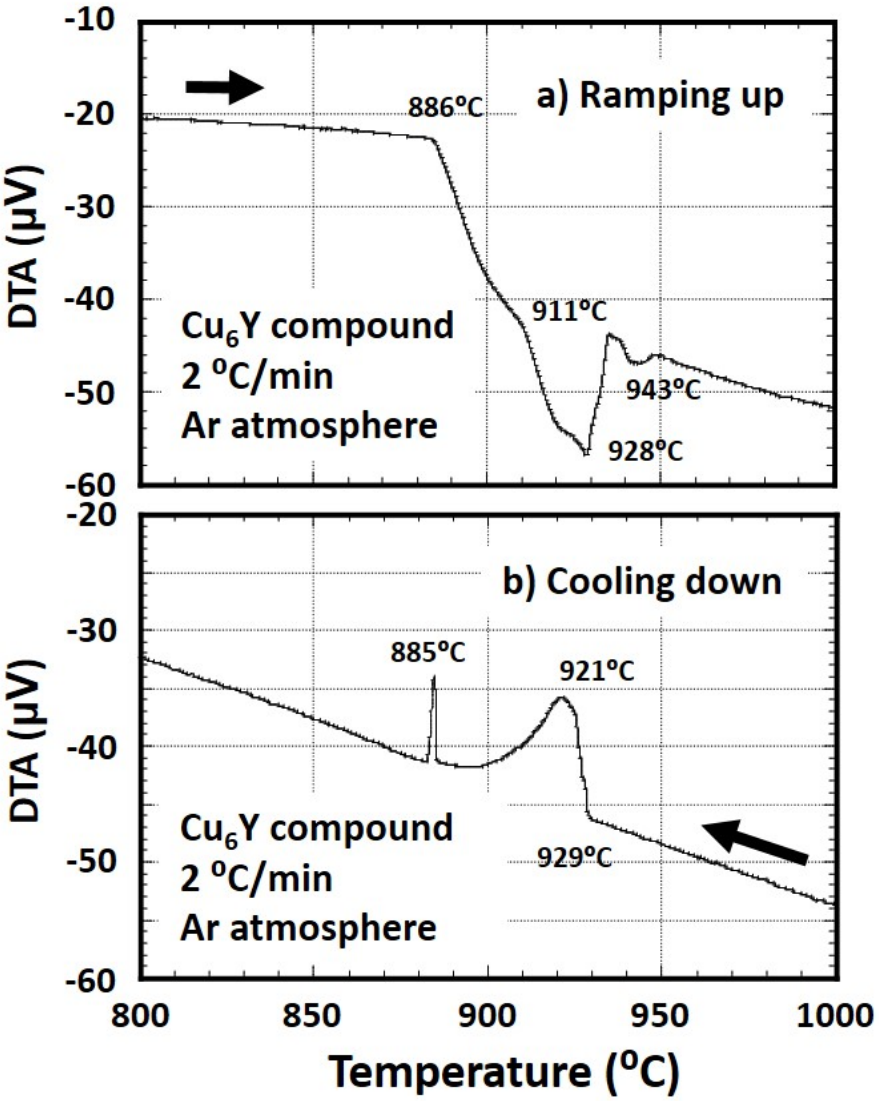

Figure.2 Bing Ma et al.

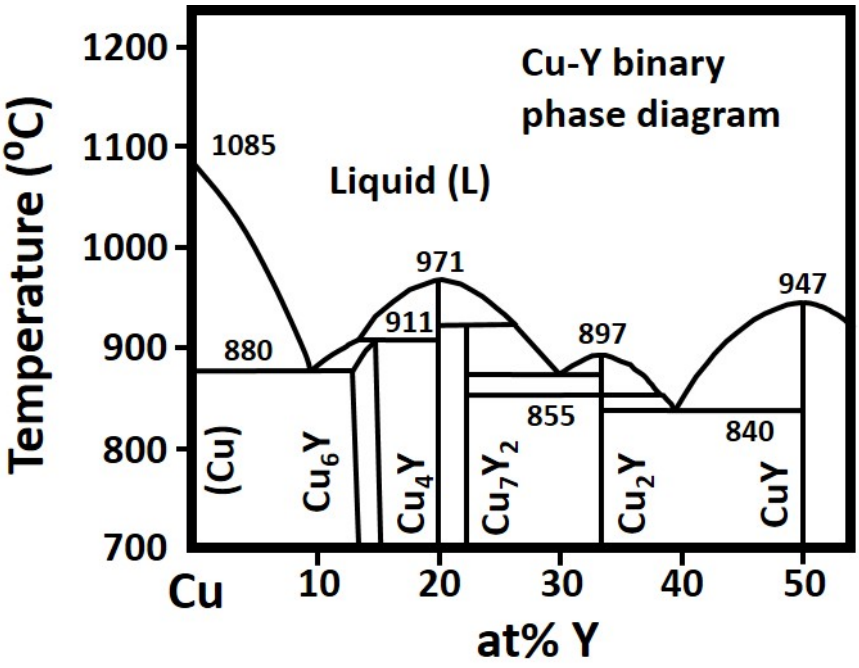

Figure.3 Bing Ma et al.

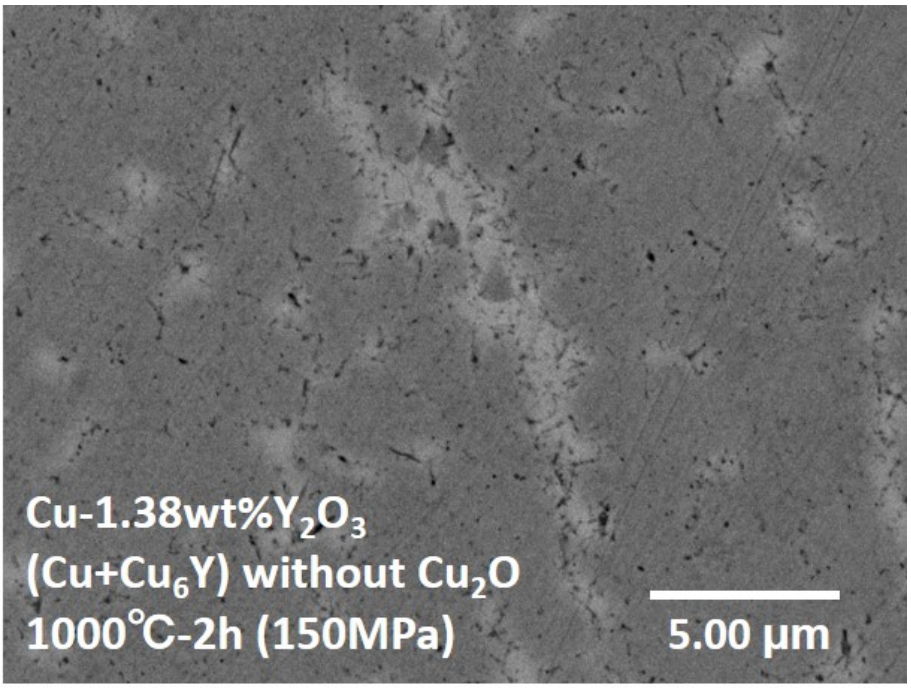

Figure.4 Bing Ma et al.

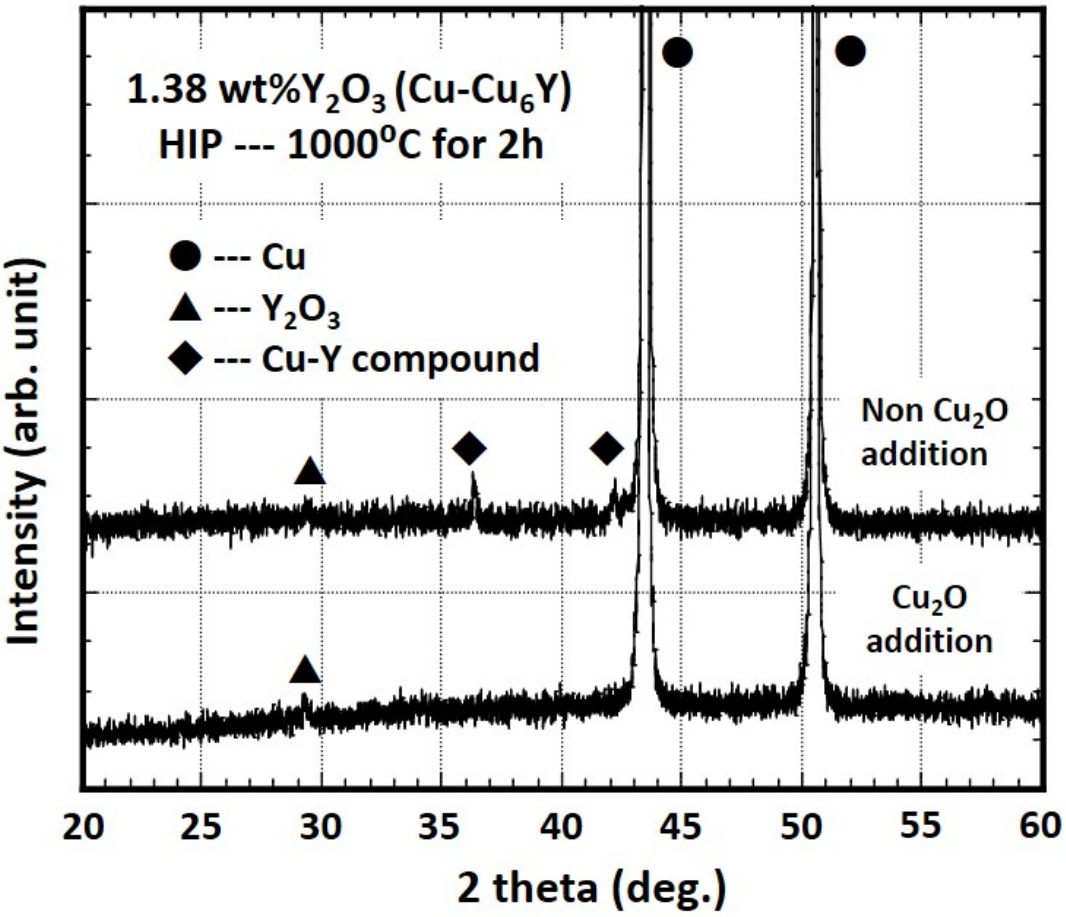

Figure.5 Bing Ma et al.

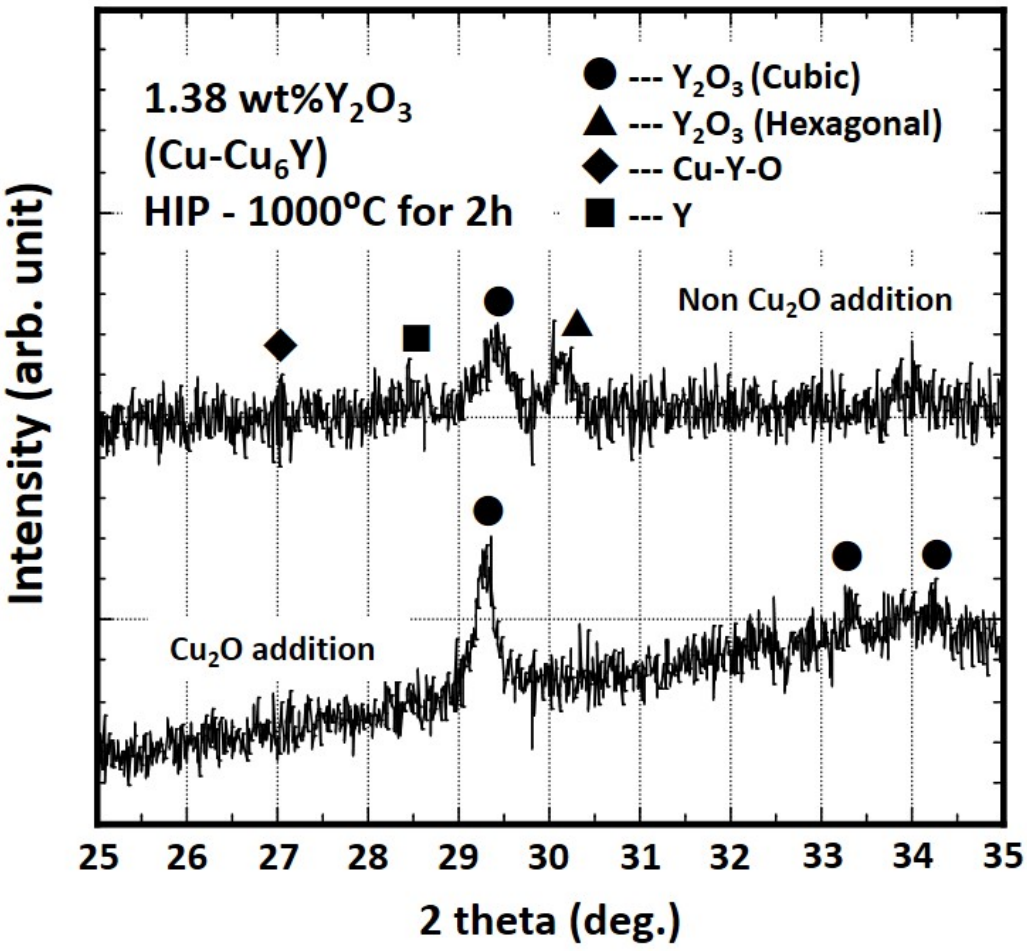

Figure.6 Bing Ma et al.

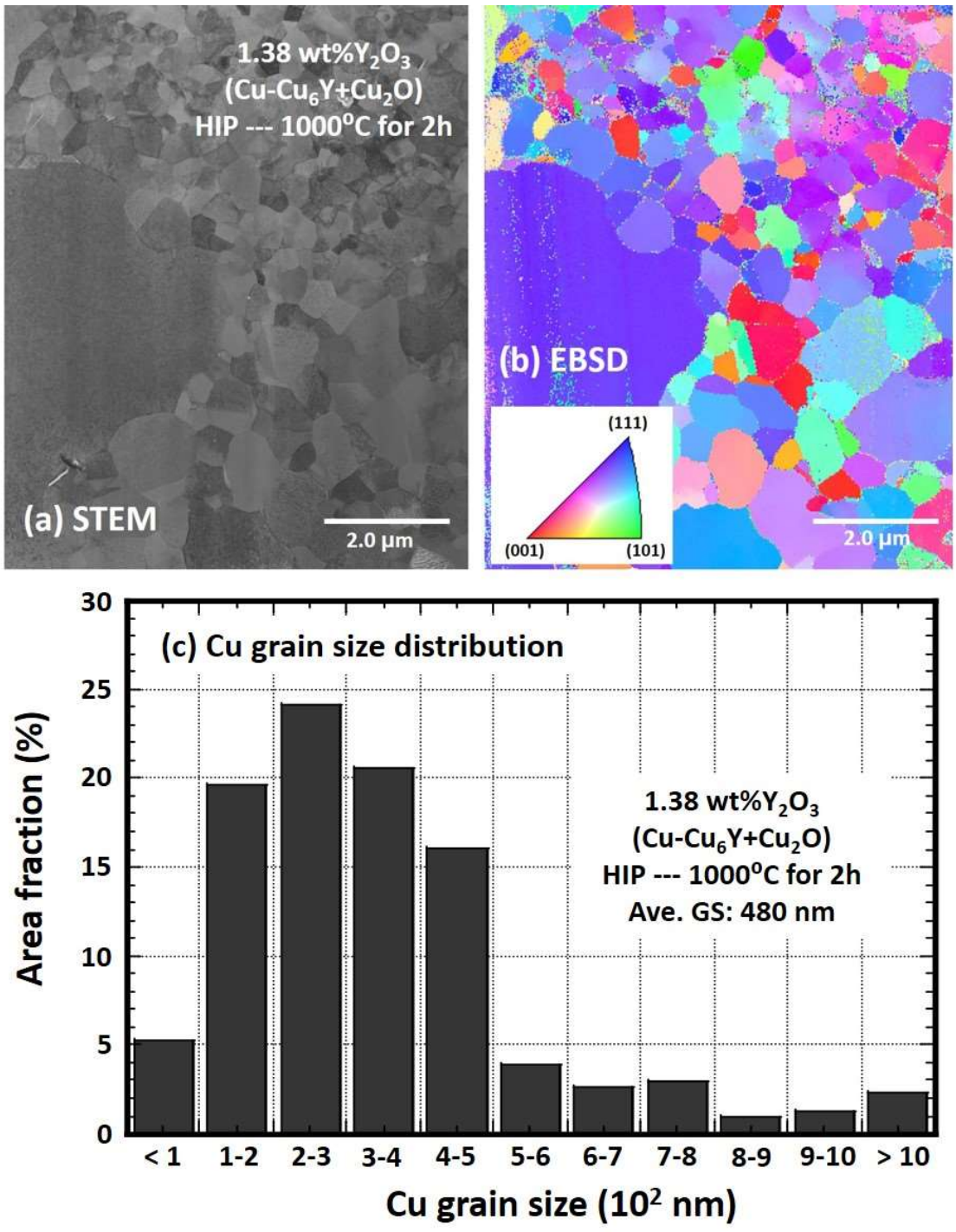

Figure.7 Bing Ma et al.

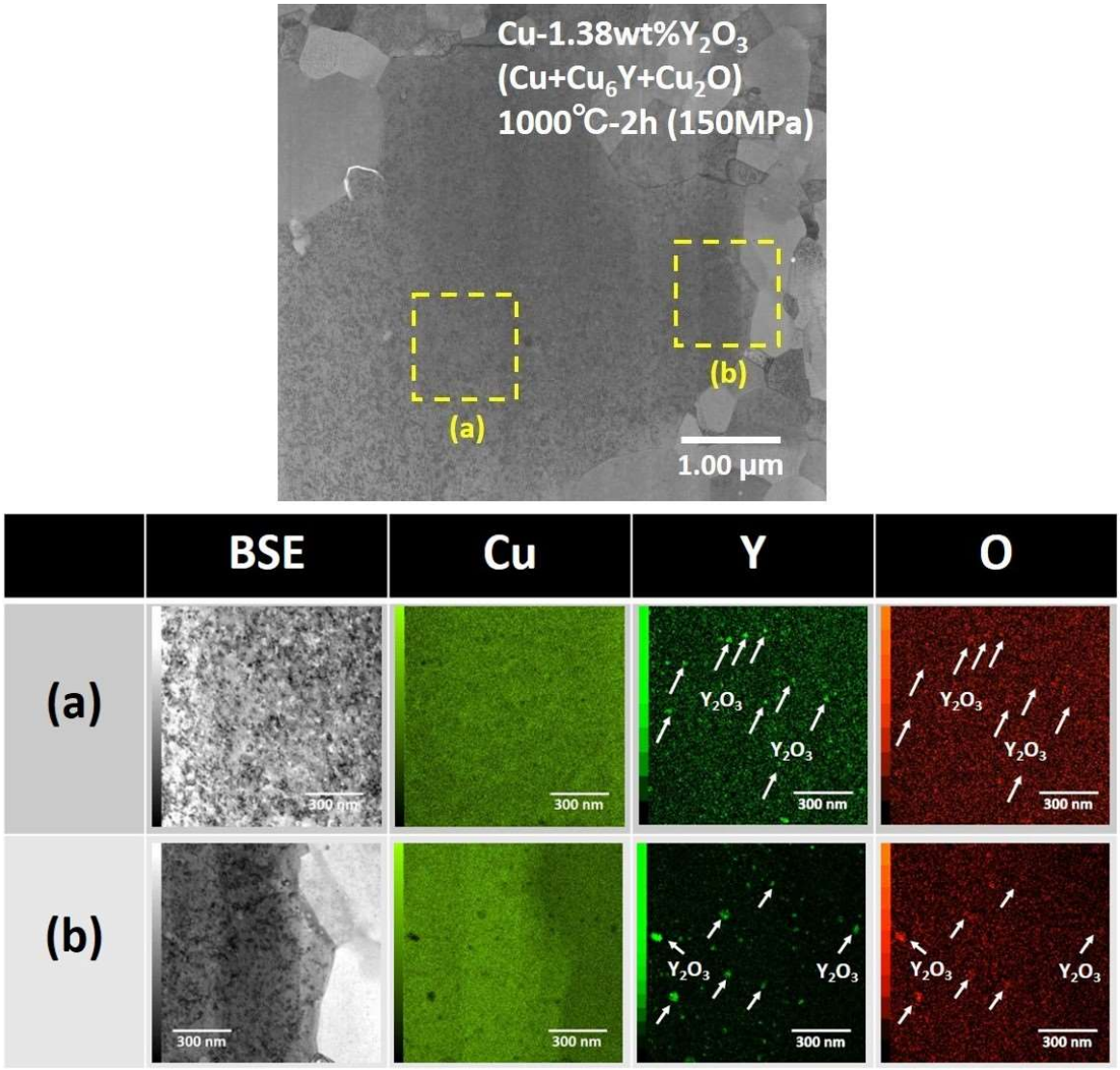

Figure.8 Bing Ma et al.

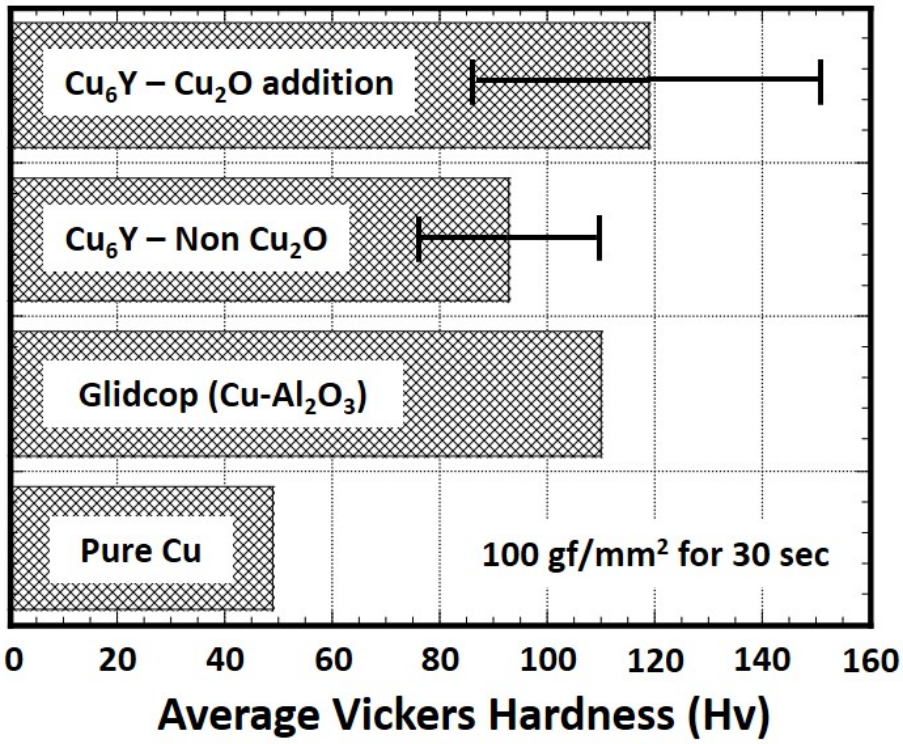

Figure.9 Bing Ma et al.